ACS APPLIED NANO MATERIALS

www.acsanm.org

Article

3D-Printed Methacrylated Gelatin–Lignin Carbon Dot Hydrogel Combined with PLA Nanofibers for Wound Dressings

Patrícia F. Rossi, Francisco Vieira dos Santos, Ana Laura Martins Mulkson Alves, Leonardo Henrique Semensato, Luis Fernando Rocha Oliveira, Danilo M. dos Santos, Tiago de Paula Bianchi, Natália M. Inada, Sérgio Paulo Campana-Filho, Rodrigo L. Oréfice,* and Daniel S. Correa*

Cite This: https://doi.org/10.1021/acsanm.4c03615

Read Online

ACCESS | Metrics & More | Article Recommendations | Supporting Information

ABSTRACT: Traditional wound dressings have limitations in terms of their antibacterial and anti-inflammatory properties, as well as their ability to maintain a moist wound environment. Addressing these deficiencies with innovative biomaterials, such as hydrogels combined with nanomaterials, can accelerate healing and perform a variety of functions in advanced biomedical materials. In this study, 3D-printed hydrogel membranes were designed and combined with nanofibrous PLA mats produced by the solution blow spinning technique (SBS) for use as a bilayered wound dressing. These membranes were manufactured from gelatin modified with methacrylamide groups (GMA), incorporated with bioactive lignin carbon dots (CDs), and cross-linked using ultraviolet (UV) light. The GMA membranes with the addition of lignin CDs showed antimicrobial activity against *Staphylococcus aureus* and *Escherichia coli* and greater mechanical deformation when combined with the PLA fibrous mats, in addition to not causing cytotoxic effects in human fibroblasts. Furthermore, the developed material was capable of maintaining a persistent hydrated environment in the wound area with adequate degradation capacity. Our results demonstrate the potential for manufacturing multifunctional wound dressings utilizing biodegradable and sustainable nanomaterials that are both cost-effective and straightforward to produce, with applications in biomedical fields, including the treatment of skin wound infections.

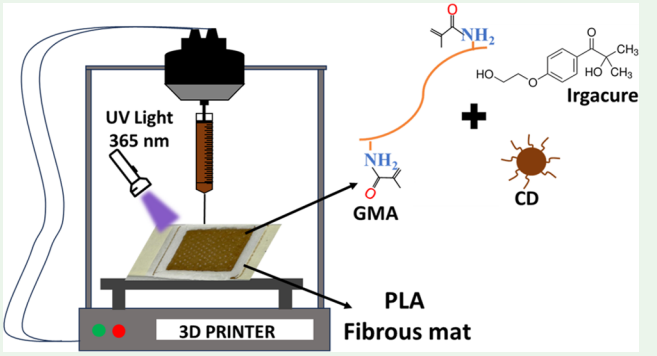

KEYWORDS: *polymers, lignin carbon dots, 3D printing, solution blow spinning, wound dressings, methacrylated gelatin, biopolymers, nanofibers*

1. INTRODUCTION

The skin has the largest surface area of any organ in the human body, performing several essential functions, such as thermal regulation and sensory functions. Moreover, it acts as a protective barrier against injuries that can damage its structure and prevent it from performing its biological functions.[1−5] Skin wounds can be superficial, reaching the subdermal layer, or deep, affecting the dermis, epidermis, and hypodermis, and can lead to infections and expose the body to other serious diseases.[6,7] In this direction, wound dressings are among the most widely used clinical treatments, as they are an accessible therapeutic intervention whose principle is to improve wound healing conditions, physically protect the affected area, reduce inflammation, and promote healing.[8,9]

Tissue engineering strategies have been proposed to develop smart and multifunctional materials for wound dressings, to provide a wound covering capable of mimicking the skin and allowing cell migration, adhesion, and proliferation.[10,11] In this context, extrusion 3D printing is a versatile additive manufacturing technology for building layer-by-layer structures,[12,13] allowing the fabrication of customized hydrogel-based devices for biomedical applications.[14−16] These hydrogels must present biological characteristics to support cell migration, adhesion, proliferation, and adequate mechanical and degradation properties.[7,11] Hydrogels based on natural polymers have been considered attractive candidates for this purpose due to their chemical, physical, and biological properties, including biocompatibility, biodegradability, and swelling capacity.[17,18] Hydrogels based on methacrylated

Received: June 27, 2024
Revised: September 23, 2024
Accepted: September 26, 2024

Scheme 1. Schematic Representation of (A) Synthesis of Methacrylated Gelatin (GMA) (A) and (B) Production of Membranes using the 3D Printing Technique using the GMA Hydrogel Combined with Lignin Carbon Dots, Which Were Deposited on the Top of PLA Fibrous Mats Produced by Solution Blow Spinning. (C) Illustration of Wound Dressing with Antimicrobial and Biodegradable Properties Applied on the Skin Wound (C).

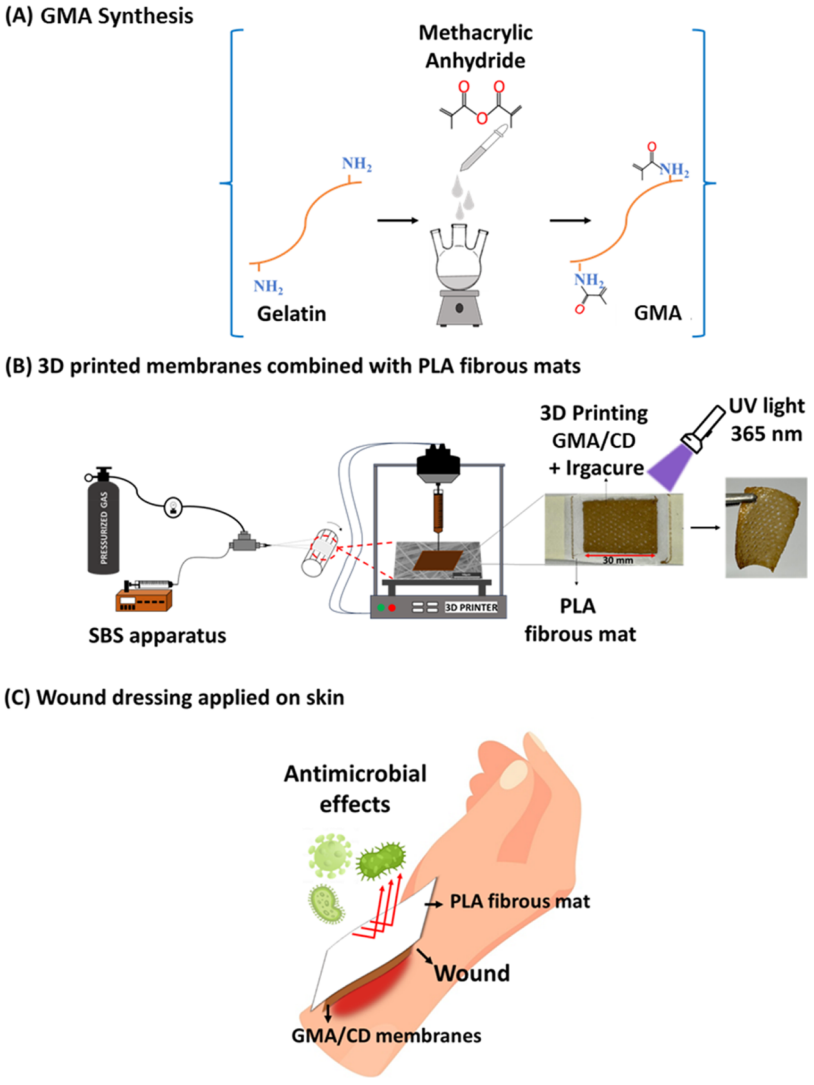

gelatin (GMA) have been employed in 3D printing,[1,10,19] where methacrylate groups are incorporated into the gelatin structure to obtain photo-cross-linked hydrogels with the aid of photoinitiators. One remarkable example of a photoinitiator is the 2-hydroxy-4′-(2-hydroxyethoxy)-2-methylpropiophenone (Irgacure 2959), which enables the cross-linking of the primary amine groups in gelatin with methacrylic anhydride (MA). GMA can be used in biomedical applications,[20−22] once it is thermosensitive and capable of mimicking the skin's extracellular matrix, being widely used in the development of dressings.[11,23]

Lignin, a natural polymer obtained as a byproduct of the cellulose and biofuels industry, is an alternative and sustainable source for obtaining carbon precursors to produce carbon dots (CDs).[24,25] CDs are synthesized from a simple and low-cost hydrothermal route,[26,27] furthermore, they exhibit unique characteristics, such as tunable photoluminescence, high fluorescence quantum yields, photostability, water dispersibility, and biocompatibility,[28] and are applied in bioimaging, biomedicine, biosensors, energy storage, and catalysis.[29−32] For instance, recently, a composite formed by poly(ether sulfone) (PES) film and a hydrogel based on ammonium persulfate, sodium p-styrenesulfonate, and N,*N*-methylenebis(acrylamide) incorporated with carbon dots (CDs) (extracted from banana peel) was demonstrated. The membrane showed anticoagulant and antioxidant properties attributed to the presence of carboxyl and hydroxyl groups in the chemical structure of CDs, which properties are suitable for hemodialysis treatment.[33]

Concerning polymers to be used for wound dressings, polylactic acid (PLA) has advantageous properties. PLA is an aliphatic thermoplastic polyester that can be produced from the condensation of lactic acid obtained from renewable sources, such as corn and sugar cane. This polymer presents biocompatibility, biodegradability,[34,35] and suitable mechanical properties, enabling the manufacturing of polymeric nanofibers by the solution blow spinning (SBS) technique for biomedical applications.[36−39]

In this context, we demonstrate the development of bilayer materials created by 3D printing and solution blow spinning

https://doi.org/10.1021/acsanm.4c03615
ACS Appl. Nano Mater. XXXX, XXX, XXX−XXX

(SBS) techniques that are potentially useful for designing multifunctional wound dressing. Specifically, we produced a PLA-based nanofibrous mat by using the SBS technique and deposited on top of it a 3D-printed GMA-based membrane incorporated with CDs. The printed GMA membrane acts as a primary layer, while the PLA-based nanofibrous mats form a secondary layer, which aims to improve the mechanical properties of the materials produced, as illustrated in Scheme 1.

2. EXPERIMENTAL SECTION

2.1. Materials. Type A porcine skin gelatin, methacrylic anhydride, dialysis membrane/MWCO 12−14 kDa, 2-hydroxy-4′-(2-hydroxyethoxy)-2-methylpropiophenone (Irgacure 2959), and chloroform was purchased from Sigma-Aldrich, and used as received. Phosphate buffered saline (PBS) 0.1 mol·L^{-1}, anhydrous sodium phosphate (Na_2HPO_4), anhydrous monobasic sodium phosphate (NaH_2PO_4), and *N*,*N*-dimethylformamide were obtained from Êxodo Cientifica (Brazil) and used as received. Kraft lignin, obtained from Ingevity, was synthesized into lignin carbon dots (CD). Poly(lactic acid) 4060D (Mn = 120,000 g·mol^{-1}) was purchased from Nature Works. For microbiological assays, Mueller Hinton agar and broth were obtained from Himedia and used as received and the antibiotic Streptomycin Sulfate was purchased from Sigma-Aldrich.

2.2. Synthesis of Lignin Carbon Dots (CDs) and Methacrylated Gelatin (GMA). Lignin CDs were synthesized using the hydrothermal method.[31] For this, 1.05 g of lignin was suspended in 35 mL of deionized water, followed by heating in a Teflon-lined stainless-steel autoclave at 180 °C for 5.5 h. Afterward, the resulting suspension was cooled to room temperature, and the supernatant was transferred to Falcon tubes for centrifugation (8000 rpm for 20 min). The supernatant was then filtered using a 0.22 μm syringe filter. Subsequently, dialysis was conducted using a membrane with a nominal molecular weight cutoff of 2000 Da for 48 h, after which the resulting CD suspension was stored at 8 °C until use and characterization.

The synthesis of GMA was conducted following the method reported in the literature with adaptation.[40] In brief, 10 g of gelatin was dissolved in 100 mL of phosphate buffer solution (PBS) at pH 7.4, utilizing vigorous magnetic stirring at 50 °C. Subsequently, 6 mL of methacrylic anhydride was added dropwise to the gelatin solution, which was maintained under stirring at 50 °C for 3 h. The reaction medium was then diluted with 300 mL of PBS previously heated to 50 °C. The resulting mixture was subsequently dialyzed for 7 days using a membrane with a nominal molecular weight cutoff of 12−14 kDa, with the dialysis water being changed at least twice per day. The GMA solution was frozen at −20 °C after the dialysis process and subjected to freeze-drying for 7 days.

2.3. Preparation of PLA Fibrous Mats and GMA Membranes. Nanofibrous mats were produced from a PLA (12% w/v) solution using $CHCl_3$/DMF in a proportion of 4:1 (v/v) under magnetic stirring, for 15 h at room temperature. The SBS experimental apparatus comprises a polymer solution injection system, a compressed air source, and a 25 mm hollow rotating collector at 180 rpm (Scheme 1B, left side). The injection system consisted of a 20 mL glass syringe, coupled to a capillary resistant to organic solvents, a 0.5 mm diameter nozzle, and an injection pump. The internal capillary was kept 2 mm away from the external nozzle. Additionally, the following parameters were fixed: (i) solution flow rate (7.5 mL/h) (ii) pressure (2 bar), (iii) working distance (22 cm), temperature (25 °C), and (iv) relative humidity (35%)

Previous tests were carried out using different concentrations of GMA (6, 8, and 10% w/v) to obtain hydrogels with ideal rheological behavior for 3D printing. Tests were also carried out with different concentrations of lignin CD (2.5, 5.0, and 10 wt %) to obtain membranes with antibacterial properties. The hydrogels were prepared as follows: first, 50 mg of Irgacure 2959 was solubilized in 5 mL of PBS at 50 °C. Then, 0.5 g of GMA was added and solubilized, after which CD was added in proportions of 5 and 10 wt %. In another beaker, 0.3 g of gelatin was solubilized at 50 °C and then mixed with the solution containing GMA/CD in a 1:1 v/v ratio. The hydrogels were named GMA, GMA/CD5, and GMA/CD10. After complete solubilization, the resulting hydrogel was transferred to a 10 mL polypropylene syringe that was cooled to 10 °C for approximately 10 min before starting the 3D printing process.

The GMA-based membranes were fabricated onto the surface of PLA fibrous mats utilizing a 3D printer (Genesis, Solutions 3D Biotechnology, Brazil), with 0.01 mm precision in the *x* and *y* axes, and 0.005 mm precision in the *z*-axis. For this purpose, structures in honeycomb format were constructed using Simplify 3D software and printed in a rectangular configuration, with dimensions of 30 mm × 22 mm × 0.5 mm, on microscope slides (76 mm × 26 mm) previously sterilized in 70% ethanol. The printing velocity was set to 3.3 m s^{-1}, with an extrusion factor of 0.10 and a 0.25 mm thickness for each of the two deposited layers using a 22G (outer diameter = 0.41 mm) polypropylene conical needle. The printing duration for producing a membrane with the aforementioned dimensions was 10 min, with a filling density of 35%. Following printing, microscope slides containing the membranes deposited on their surfaces were placed in a UV light cabinet (Biothec BT 107/UV 15 W) and exposed to λ = 365 nm UV radiation for 30 min to carry out the cross-linking reaction. The resulting membranes were designated as PLA/GMA, PLA/GMA/CD5, and PLA/GMA/CD10 for materials containing no lignin CD and 5 and 10 wt % of lignin CD, respectively.

2.4. Rheological Characterization. Rheological tests were conducted to predict the behavior of hydrogels in terms of their viscoelastic, pseudoplastic, and thixotropic properties during the 3D printing process, as well as to evaluate the impacts of incorporating lignin CD into hydrogels GMA/CD5% (w/v), and GMA/CD10% (w/v). For this, the rheological profiles of the hydrogels were evaluated at 25 °C using the rotational rheometer DHR-2 (TA Instruments) with cone−plate geometry, with a gap of 55 μm, diameter of 40 mm, and cone angle of 2°. Flow sweep was performed to generate viscosity curves within the range of shear rate from 0.1 to 1000 s^{-1}. Oscillation amplitude was conducted at a constant angular frequency of 10 rad s^{-1} within the range of strain from 0.01 to 1000%, while oscillation frequency was performed at a constant strain of 1.0% with angular frequency in the range of 0.1 to 100 rad s^{-1}. The oscillation temperature ramp was conducted within the temperature range from 25 to 45 °C with a heating rate of 5 °C min^{-1}. Additionally, the thixotropy of the samples was evaluated using three sequential steps of flow peak hold. In the first step, the shear rate was constant at 0.1 s^{-1} for 120 s, in the second step, the shear rate was 100 s^{-1} for 30 s, and in the final step, the initial shear rate (0.1 s^{-1} for 120 s) was recovered. All experiments were performed in triplicate.

2.5. Nuclear Magnetic Resonance Spectroscopy. The chemical structure of gelatin and GMA was determined from ^{1}H NMR analysis (AVANCE III 600 M, Bruker, Germany), and the average degree of methacrylation of GMA was calculated according to eq 1, which relates the intensity of the acrylic hydrogen signal (5.42 ppm) to the intensity of the free lysine signal (2.97 ppm), according to the procedure described in the literature.[40]

$$\text{degree of methacrylation (DM)} = \frac{I_{5.42}}{I_{5.42} + I_{2.97}} \times 100\% \quad (1)$$

2.6. Attenuated Total Reflectance Fourier Transform Infrared Spectroscopy (ATR-FTIR). The composition of GMA and the functional groups present in the structures of the produced materials were investigated by ATR-FTIR (PerkinElmer Spectrum 1000 with Spectrum software) equipped with an attenuated total reflection apparatus, employing a zinc selenide crystal. The spectra were obtained in the spectral region between 4000 and 600 cm^{-1}, accumulation of 32 scans and a resolution of 2 cm^{-1}.

2.7. Scanning Electron Microscopy (SEM). To evaluate the morphology of the membranes, a Scanning Electron Microscope (JEOL JSM-6510) was used, operating at 5 kV. To this end, small pieces of each sample were previously placed on carbon adhesive tape over aluminum stubs and then coated with a thin layer of gold using a

https://doi.org/10.1021/acsanm.4c03615
ACS Appl. Nano Mater. XXXX, XXX, XXX−XXX

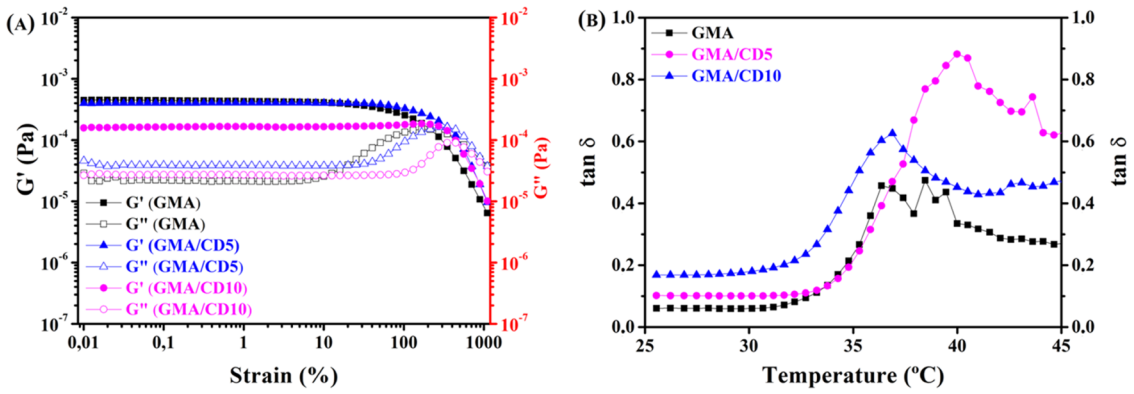

Figure 1. Rheological analysis of GMA, GMA/CD5, and GMA/CD10 hydrogels. (A) Amplitude sweeps curves for G' and G'' as a function of shear. (B) Tanδ curves as a function of temperature.

sputter coater (Leica Microsystems EM SCD050). Three different micrographs were taken of each sample.

2.8. Tensile Testing. The mechanical properties of the membranes printed on the PLA fibrous mat (GMA, GMA/CD5, and GMA/CD10) were evaluated through tensile tests carried out using dynamic-mechanical analysis (DMA Q800) adapted to the tensile mode of the thin film. The membranes were cut with a length of 7 mm, width of 5.5 mm, and thickness of 0.51 ± 0.05 mm. The tensile tests were carried out in uniaxial tension with a ramp of 0.01 N min^{-1}, preload force of 0.001 N, and strain amplitude of 0.1% in the temperature range of 25 to 30 °C.

2.9. Swelling Test. The swelling ratio (S_R%) of the membranes was evaluated by analyzing the absorption capacity in PBS. Approximately 6 mg of each membrane was immersed in vials containing 10 mL of PBS (pH = 7.4). The mass of the membranes was measured after certain periods and, before each weighing, the membranes were dried with filter paper to remove excess PBS. The swelling ratio (SR%) was then calculated from eq 2.[41,42]

$$S_{R(\%)} = \frac{w_t - w_0}{w_0} \times 100 \quad (2)$$

where w_0 and w_t are the initial sample mass and the sample mass at time t, respectively. All experiments were performed in triplicate.

2.10. Material Stability in PBS. Rectangular-shaped membrane specimens were frozen at −20 °C, freeze-dried, weighed, and placed in 10 mL glass flasks containing 5.0 mL of PBS (pH = 7.4). The vials containing the samples were incubated at 37 °C for periods of 24 and 48 h. After these periods, the samples were removed from the buffer, washed with deionized water, freeze-dried at −20 °C for 24 h, and weighed. The tests were performed in triplicate and the percentage of remaining mass ($RM_{(\%)}$) was calculated according to eq 3

$$RM_{(\%)} = \frac{w_t}{w_0} \times 100 \quad (3)$$

where w_0 is the initial weight of the material, and w_t is the weight after degradation.

2.11. Disk Diffusion Antimicrobial Testing. *Staphylococcus aureus* (ATCC 25923) was grown on tryptic soy agar (TSA) containing 6 $g{\cdot}L^{-1}$ yeast extract and *Escherichia coli* (ATCC-25922) was grown on nutrient agar (NA). Cultures were grown overnight at 37 °C. After incubation, individual colonies were suspended in fresh Müeller Hinton broth (MHB), and batch cultures were grown for 24 h at 37 °C and 150 rpm in Erlenmeyer flasks. Cultures were initially diluted in fresh MHB to approximately 5×10^8 CFU/mL to ensure that the cultures were in the exponential growth phase.

The antimicrobial activities of the membranes against *S. aureus* and *E. coli* were determined by the disk diffusion method (CLSI, 2018). To this end, 25 μL of each membrane precursor hydrogel was applied to filter paper discs (5 mm) on the surface of streaked MHB agar plates with the bacterial suspension adjusted to the 0.5 McFarland standard (10^8 CFU/mL). Filter paper discs (5 mm) impregnated with 20 μL of streptomycin sulfate (13 $mg.mL^{-1}$) were used as a positive control and filter paper discs (5 mm) impregnated with 20 μL of MHB broth were used as a negative control. Plates were incubated at 37 °C for 24 h before reading.

2.12. Cytotoxicity Assay. Cytotoxicity experiments were conducted using a neonatal Human Dermal Fibroblast cell line (HDFn - Gibco #CC0045C). These cells are derived from the neonatal foreskin and are commonly used in a variety of research areas, including studies related to skin aging, skin diseases, and wound healing.[43−45] The cells were cultured in Dulbecco's modified Eagle's medium (DMEM) supplemented with 10% (v/v) fetal bovine serum (FBS), and maintained in 75 cm^2 culture flasks, inside a humidified incubator at 37 °C with 5% CO_2. The culture medium was refreshed three times a week and subculture was performed when the confluence attained 90%, following the recommended protocol consisting of rinsing once with PBS at pH 7.4, separating cells from the flask using trypsin 0.25% (w/v) - EDTA 0.53 mM, and adding DMEM supplemented with FBS for trypsin inactivation.

The cytotoxicity was measured with a recommended test from ISO 10993-5/2009 named MTT assay. In this colorimetric analysis, the mitochondrial activity of viable cells reduces a yellow salt (MTT) to purple crystals (formazan) due to the activity of mitochondrial reductases. Therefore, this assay is an indirect method to evaluate cellular metabolic activity, *i.e.*, cytotoxicity.[46] To test the potential cytotoxicity of the material with GMA, extracts were obtained by incubating one UV-sterile square membrane sample of 1 cm^2, in 2.5 mL of DMEM 10% FBS. After 24 and 48 h of samples soaked in DMEM, membrane extracts were obtained by collecting the exposed medium and discarding the matte sample. In these experiments, cells were seeded into 96-well plates, 1×10^4 cells per well in 200 μL, 24 h before being exposed to membrane extracts. After this interval, the cells were incubated for 24 h with 200 μL medium extracts previously exposed to PLA/GMA, PLA/GMA/CD5, or PLA/GMA/CD10 membranes. The control group was incubated with DMEM 10% FBS, without being exposed to any membrane samples. Subsequently, the extracts were removed from the cells and 100 μL of MTT (3-(4,5-Dimethylthiazol-2-yl)-2,5-Diphenyltetrazolium Bromide) at 0.5 $mg{\cdot}mL^{-1}$ in DMEM was added to each well, followed by 3 h of incubation at 37 °C with 5% CO_2. Then, the medium was removed and 100 μL of DMSO was added to dissolve the formazan crystal. The absorption was measured using a microplate reader (Multiskan FC Microplate Photometer, #51119000) at 570 and 690 nm. The relative metabolic activity was calculated by normalizing the absorption values, to define the absorption of the control groups, that is, the relative metabolic activity at 100%. Three independent experiments were performed in quintuplicate. The results were presented as mean ± standard deviation and each group had a sample size of $n = 15$. Kolmorog-Srminov test verified the normality of data as the variance was analyzed using the One-Way ANOVA test, with

https://doi.org/10.1021/acsanm.4c03615
ACS Appl. Nano Mater. XXXX, XXX, XXX−XXX

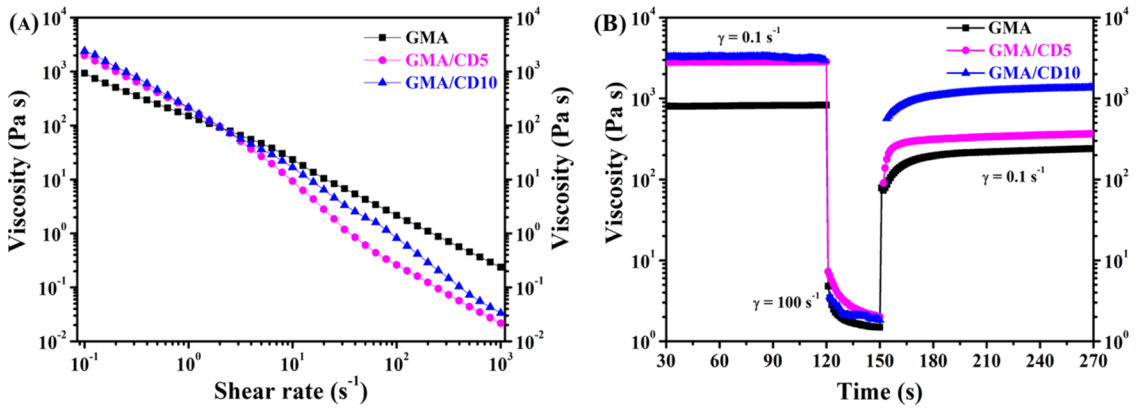

Figure 2. Rheological characterization for GMA, GMA/CD5, and GMA/CD10 hydrogels. (A) Flow sweep curves for viscosity as a function of shear. (B) Viscosity recovery curves as a function of time.

group means compared by the Tukey test, both with a significance level of 0.05.

3. RESULTS AND DISCUSSION

3.1. Rheological Analysis. The viscoelastic behavior of hydrogels for 3D printing can be evaluated by the determination of the storage (G') and loss (G'') moduli as a function of strain or stress.[47,48] This allows obtaining information about the contribution of both elastic and viscous behavior, attributed respectively to G' and G'',[49] that constitute the three-dimensional polymeric network present in the hydrogels formed through physical or chemical cross-linking.[50]

Figure 1A shows the behavior of G' and G'' (amplitude sweep) for the GMA, GMA/CD5, and GMA/CD10 hydrogels as a function of the strain. It was possible to determine the linear viscoelastic region (LVR), where for all tested hydrogels G' and G'' remain constant, showing that the hydrogels have characteristics of solid materials ($G' > G''$). On the other hand, outside the LVR, G' and G'' are affected by deformation and the hydrogels have a flow point ($G' = G''$), indicating that they are capable of flowing under deformation, which is a desired behavior for materials used in 3D printing. This result shows that the proposed hydrogels can manufacture materials using the 3D printing technique. Still, in Figure 1A it is possible to notice that the flow point of the GMA hydrogel occurred at 272%, followed by GMA/CD5 at 357% and GMA/CD10 at 467%. This result also shows that incorporating CD into the hydrogels affected their flow point.

We also evaluated the behavior of the hydrogels as a function of the temperature. The parameter tan δ or damping coefficient, defined as the ratio between G'' and G', can predict whether the hydrogels behave as an elastic solid or viscous fluid.[51] When tan $\delta < 1$ the hydrogel behaves like an elastic solid (gel), for tan $\delta > 1$ the hydrogel behaves like a viscous fluid (liquid), while tan $\delta = 1$ indicates that the polymer network present in the hydrogel is in the transition phase between the gel and liquid state.[52] Figure 1B shows the behavior of tan δ as a function of temperature for the GMA, GMA/CD5, and GMA/CD10 hydrogels. It is noted that for temperatures below 30 °C, the hydrogels are in the gel state, however, above 30 °C it is noticed that the value of tan δ begins to increase, showing that the polymeric network present in the hydrogels is partially disassembled. For the GMA, GMA/CD5, and GMA/CD10 hydrogels, the maximum tan δ values were 0.46, 0.88, and 0.62 respectively. This result indicates that the presence of CD changed the behavior of tan δ in a nonlinear way. Furthermore, it suggests that the polymeric network present in the GMA/CD5 hydrogel has been disrupted to a greater extent than those of the other hydrogels, showing that GMA/CD5 has a more viscous character as compared to the other hydrogels. On the other hand, from 37 °C the value of tan δ is reduced for the GMA hydrogels and GMA/CD10, while for GMA/CD5 this reduction occurred from 40 °C onward. This shows that all hydrogels have a certain capacity to remake the polymeric network even after increasing the temperature. The temperature sweep results provide important information about the behavior of the polymer network present in the hydrogels, which can be useful for processing materials through the 3D printing technique.[53,54]

Hydrogels used to produce materials through the 3D printing technique need to flow under shear.[55] In this sense, we evaluated the pseudoplastic behavior of GMA, GMA/CD5, and GMA/CD10 hydrogels through flow sweep, which allowed us to understand the hydrogels' ability to flow under shear.

In Figure 2A, the viscosity behavior of the hydrogels as a function of the shear rate is observed. Initially, GMA/CD5 and GMA/CD10 have viscosity values of 930, 1985, and 2401 Pa s^{-1}, respectively, and by increasing the shear rate to 1000 s^{-1}, it is noted that the viscosity of the hydrogels is drastically reduced, suggesting that the applied shear disrupts the polymeric network present in the hydrogel. This behavior is desired for hydrogels used in 3D printing,[23] as during the printing process the hydrogel needs to flow through the needle to be deposited on a given surface/substrate.

The results of the flow sweep showed that the GMA, GMA/CD5, and GMA/CD10 hydrogels are capable of flowing under shear, the presence of CD increased the viscosity of the GMA/CD5 and GMA/CD10 hydrogels, however, from the shear rate of 10 s^{-1}, it was observed that the hydrogels showed greater viscosity reduction when compared to the GMA hydrogel. This behavior suggests that the incorporation of CDs causes the GMA/CD5 and GMA/CD10 hydrogels to have a more pronounced pseudoplastic character.

Another important test in the development of hydrogels for 3D printing is the evaluation of thixotropy, which aims to determine the ability of the hydrogel to recover viscosity as a function of time.[52,53] During the 3D printing, three stages characterize the hydrogel 3D printing process. The first one is characterized by the formation of the hydrogel inside the

https://doi.org/10.1021/acsanm.4c03615
ACS Appl. Nano Mater. XXXX, XXX, XXX−XXX

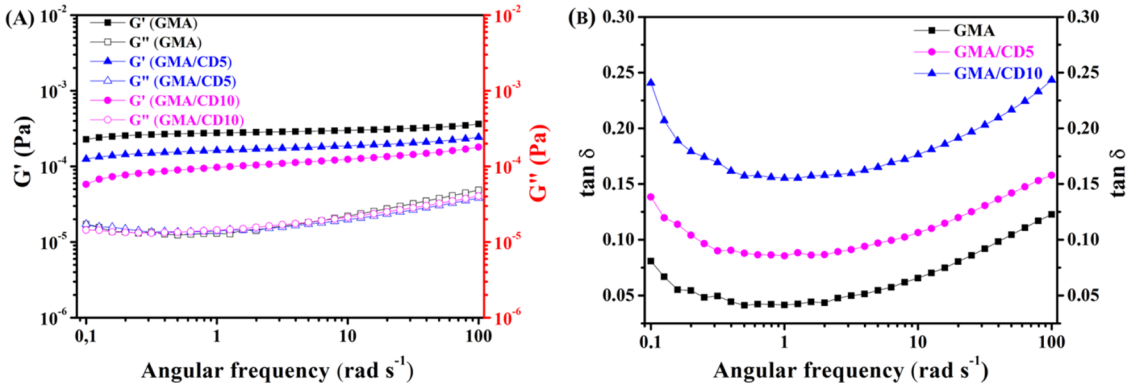

Figure 3. Rheological evaluation for GMA, GMA/CD5, and GMA/CD10 hydrogels. (A) Frequency sweep curves for G' and G'' as a function of shear. (B) tan δ curves as a function of frequency.

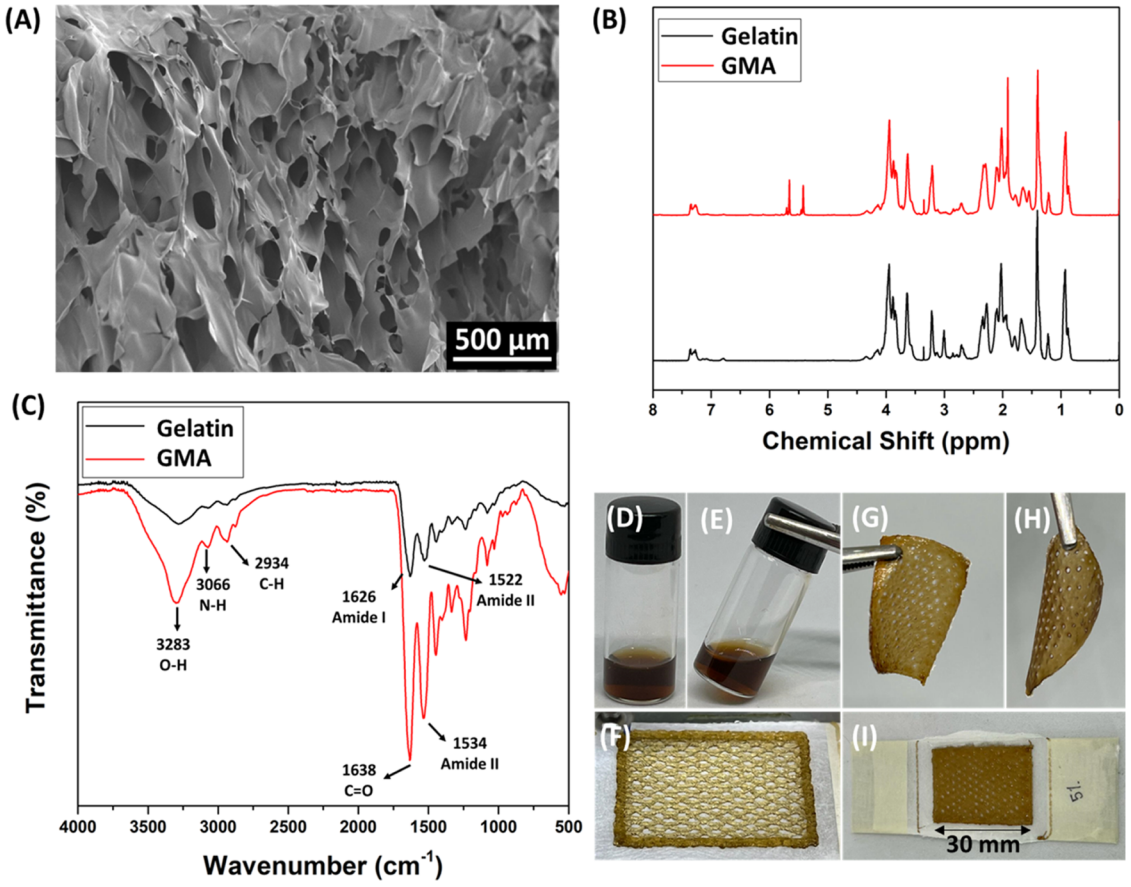

Figure 4. (A) SEM micrographs of GMA. (B) NMR spectroscopy of GMA and Gelatin. (C) FTIR spectra of Gelatin and GMA. (D) and (E) GMA hydrogel containing lignin-derived carbon dots after preparation at 50 °C. (F) Printed structure of GMA with lignin carbon dots hydrogel. (G) and (H) Hydrogel membranes after cross-linking by UV light at λ = 365 nm for 30 min (I) GMA/CD-based membrane printed on PLA nanofibers produced by SBS.

syringe. In the second stage, the hydrogel's polymer network is disrupted by the shear action during printing, which causes it to flow and be deposited on the work surface. Finally, in the third stage after being deposited, the hydrogel needs to reassemble its polymeric network broken by shear, as well as recover the initial viscosity and consequently return to the solid state (gel) over time.[56] The higher this viscosity recovery, the higher the hydrogel's ability to allow the fabrication of structures with remarkable shape retention.[57] To this end, we monitored the viscosity recovery of the GMA, GMA/CD5, and GMA/CD10 hydrogels as a function of time, first applying a shear of 0.1 s^{-1} for 120 s, then increasing the shear to 100 s^{-1} for 30 s and finally applying again shear of 0.1 s^{-1} for 120 s, as shown in Figure 2B. It is observed that at a low shear rate (0.1 s^{-1}) the viscosity of the hydrogels does not suffer reduction, however increasing it to 100 s^{-1} we notice that the viscosity value reduces drastically for all hydrogels because at this shear rate, the network polymer is broken down and consequently the viscosity is reduced, characterizing a pseudoplastic behavior. Resuming the initial shear of 0.1 s^{-1} and waiting a certain time, it is observed that the hydrogels are capable of recovering a certain part of the polymeric network disrupted by

https://doi.org/10.1021/acsanm.4c03615
ACS Appl. Nano Mater. XXXX, XXX, XXX−XXX

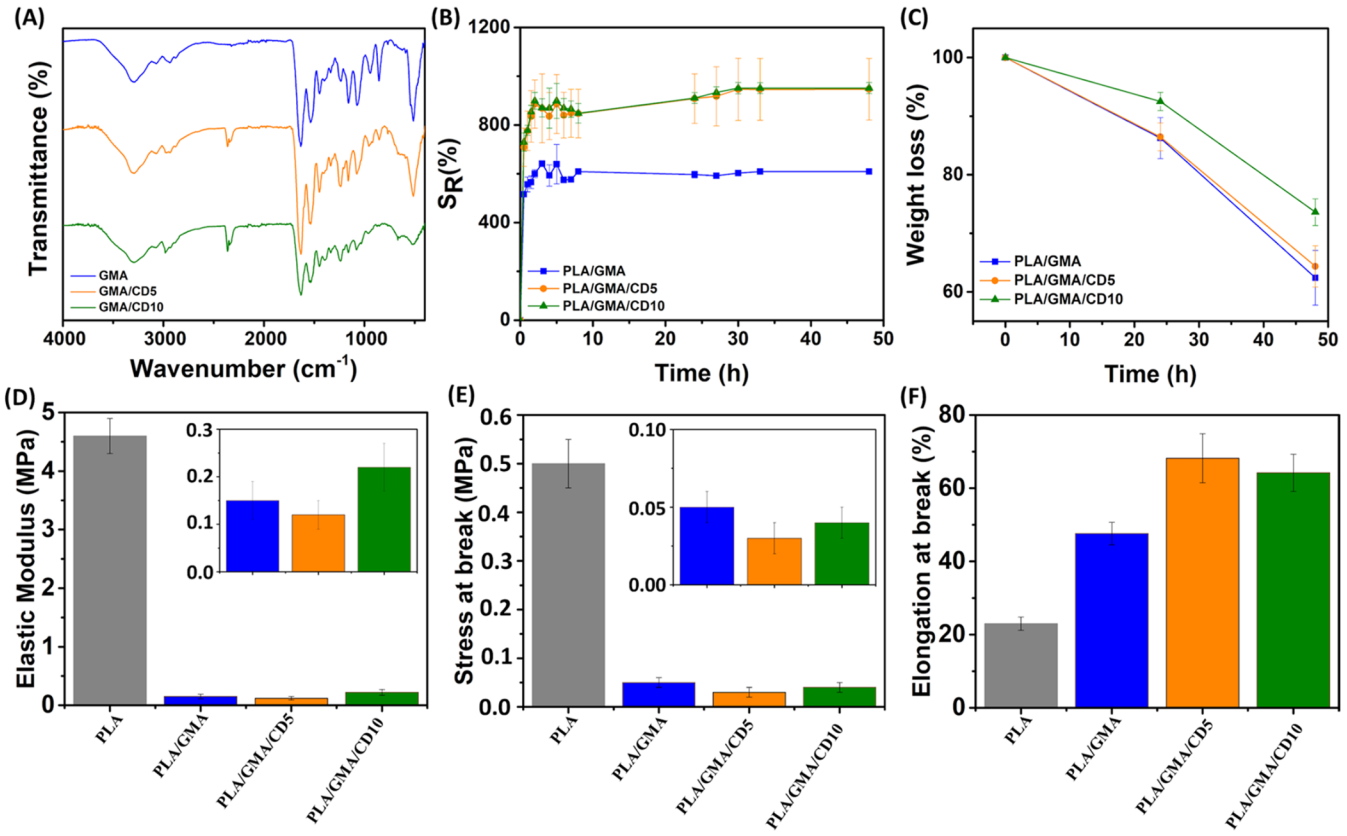

Figure 5. (A) FTIR spectrum of GMA, GMA/CD5 and GMA/CD10 membranes. (B) Degree of swelling of PLA/GMA, PLA/GMA/CD5, and PLA/GMA/CD10 membranes. (C) Susceptibility to degradation of PLA/GMA, PLA/GMA/CD5, and PLA/GMA/CD10 membranes. Mechanical properties of DMA tensile, (D) Modulus of elasticity (E) Stress at break, and (F) Elongation at break.

the shear, and with this, the viscosity increases (thixotropy), which behavior is important for hydrogels used in 3D printing.[23] It is also noted that the GMA/CD10 hydrogel displayed the highest recovery compared to the other hydrogels. These results show that incorporating 10% m/m of CD in the hydrogel favored viscosity recovery compared to the GMA hydrogel. Furthermore, it was possible to monitor this viscosity recovery at the time of printing, right after the hydrogel left the needle and was deposited onto the work surface.

Finally, we performed a frequency sweep within the LVR to evaluate the behavior of G' and G'', as well as tan δ as a function of frequency, as can be seen in Figure 3A,B. It can be seen in Figure 3A that in the frequency range from 0.1 to 100 rad s^{-1} GMA, GMA/CD5, and GMA/CD10 hydrogels presented, $G' > G''$. This result shows that the hydrogels are predominantly elastic, indicating their suitability for 3D printing. Furthermore, Figure 3B corroborates the result presented, as for the entire frequency range analyzed, the value of tan δ was lower than 1, confirming that the hydrogels behave like gels.

3.2. Microstructural Analysis. Microstructural characteristics of GMA after the synthesis process and subsequent freeze-drying were investigated using images obtained by SEM analysis. In Figure 4A, the micrograph shows the internal microstructures of GMA and the presence of irregular and asymmetrical pores resulting from the freezing process.[58]

^{1}H NMR spectroscopy was used to confirm the insertion of methacrylic moieties in the gelatin structure and determine the average degree of substitution. Each of the functional groups in the gelatin polypeptide structure, comprising hydroxyl, amino, and carboxyl groups, can react with methacrylic anhydride, resulting in a photo-cross-linkable prepolymer.[1] The different proportions of gelatin and methacrylic anhydride can result in hydrogels with variable mechanical characteristics, as well as swelling and biodegradability profiles.[11] Figure 4B represents the ^{1}H NMR spectra of gelatin and GMA with a wide number of amino acid signals. An increase in the intensity of the methyl group signal (δ = 1.8 ppm), a decrease in the intensity of the free lysine signal (δ = 2.9 ppm),[59] and the appearance of two new acrylic hydrogen signals (δ = 5.4 and 5.6 ppm), which are attributed to acrylic hydrogen in the GMA spectrum confirms the success of gelatin methacrylation.[60] Using eq 1, which makes a relationship between the intensity of signals at ∼5.42 and ∼2.97 ppm, it was possible to determine the average degree of methacrylation of GMA as 53.7%.[40]

Fourier transform infrared spectroscopy (FTIR) was performed to verify the effectiveness of dialysis in removing residues from the synthesis. Figure 4C presents the spectra obtained from the non-cross-linked GMA/gelatin matrix. In the spectra, it is possible to observe a broad band at 3284 cm^{-1}, attributed to the O−H and N−H stretching vibrations, and two bands between 2870 and 2943 cm^{-1} denoting the C−H stretching of the $-CH_2$ groups and tertiary groups −CH present in the functional groups of gelatin and methacrylate.[59,60] The main structure of gelatin is denoted by bands at 1630 cm^{-1}, referring to stretching of the amide group I, (C═O), 1534 cm^{-1}, referring to the amide group II (N−H bending), and 1239 cm^{-1}, referring to amide III (stretching (C−N)).[61] There are no strong bands between 1690 and 1760

https://doi.org/10.1021/acsanm.4c03615
ACS Appl. Nano Mater. XXXX, XXX, XXX−XXX

cm^{-1}, characteristic of methacrylate anhydride, referring to the carbonyl group (C═O), indicating that the postreaction residues of this substance were completely removed from GMA.[62]

Figure 4D,E show the mixture of GMA and lignin carbon dots for preparing the ink at 50 °C. After this preparation, the hydrogel was transferred to a syringe and cooled until it reached a gelatinous consistency to then begin the printing process. Figure 4F shows the process during printing, while Figure 1G,H show the membrane after 30 min of exposure in a UV light cabinet (at 365 nm). Figure 1I shows how the GMA with lignin carbon dots membrane was 3D-printed onto PLA mats. Besides, in the Supporting Information one can observe the TEM image of CDs in Figure S1A, while the inset in this image shows a High-Resolution TEM image of an individual CD. Figure S1B shows the UV−vis absorption spectrum of the CDs, while the photoluminescence spectrum of lignin CDs is shown in Figure S1C.

3.3. ATR-FTIR Analysis. In the FTIR spectra Figure 5A, the presence of gelatin in the hydrogels was highlighted by the existence of absorption bands at 3297 and 3073 cm^{-1} related to the NH group.[19] It is also possible to observe, at 1635 cm^{-1} a band typical of the C═O bond, characteristic of amide I, and absorbance bands at 1540 and 1237 cm^{-1} related to amides II and III, respectively. The band related to the CH group was also observed at 1443 cm^{-1}. Absorption bands associated with methacrylic anhydride can be seen in the spectra of the hydrogels (Figure 5A) at 1070 cm^{-1} due to CO bonds.[63] Methacrylic anhydride reacts with the primary amine groups in gelatin to lead to the addition of methacrylic groups to the gelatin macromers.[60] Cross-linking of GMA occurs in the presence of a photoinitiator, which when exposed to UV light radiation produces free radicals, and GMA is then cross-linked.[64] Furthermore, Figure 5A shows bands between 2369 and 2333 cm^{-1} referring to the presence of Lignin Carbon dots in the GMA/CD5 and GMA/CD10 membranes, which are related to the axial deformations of the aliphatic chains CH_2 and CH_3.[65]

3.4. Swelling Test. Determining the swelling ratio of hydrogels is important once it is related to the ability to absorb exudate, especially in skin wounds with a high exudate content.[66] In general, the swelling ratio depends on the pore size of the hydrogel and hydrophilic behavior, which is determined by the degree of methacrylation, concentration of carbon dots, photoinitiator, and curing time. Furthermore, this ratio may be able to control the diffusion and elimination of nutrients and waste, respectively.[23] The results of the swelling ratio of the samples are shown in Figure 5B, which shows that the swelling ratios of PLA/GMA, PLA/GMA/CD5, and PLA/GMA/CD10 were 641.3, 946.5, and 951.5%, respectively, reaching equilibrium after 24 h.

Although studies on porosity were not reported in this work, the results indicate that the incorporation of CDs into hydrogels led to a possible reduction in hydrogel density and a pore reduction compared to PLA/GMA, or else the high hydrophilicity of the CDs may have enhanced greater water absorption, therefore, resulting in higher swelling behavior. According to Figure 5B, varying the concentration of CD from 5 to 10 wt % does not significantly affect the swelling of the PLA/GMA/CD5 and PLA/GMA/CD10 membranes.[1] The value obtained for the PLA/GMA membrane was similar to the value reported by Ravikumar, 2017 and Xu, 2023,[11,67] indicating that PLA/GMA/CD5 and PLA/GMA/CD10 membranes have higher water absorption capabilities than other materials for periods longer than 24 h.

3.5. Material Stability in PBS. The degradation of a material used as a skin dressing, ideally, should occur in a controlled manner, allowing the necessary time for the healing process to evolve.[68] Besides, it should ensure that at the end of this process, there are no traces of the material used as a dressing in the wound area.[69] The main proteolytic enzyme involved in wound healing is collagenase type II (matrix metalloproteinase-8 [MMP-8])[70] and, based on the literature, it is known that GMA is degraded by this enzyme since gelatin contains sequences that collagenases can recognize.[71] Figure 5C presents the degradation study of membranes obtained from 3D printing on PLA mats, in the absence of enzymes. The *in vitro* results of the present work showed that the membranes degrade rapidly from the second day of incubation (Figure 5C). The mass loss of the PLA/GMA, PLA/GMA/CD5, and PLA/GMA/CD10 membranes over 48 h are 37.6, 35.6, and 26.4%, respectively, which indicate loss only of the hydrogel, maintaining the mass of the fibrous mats that do not degrade during this period.

3.6. Tensile Test. GMA-based hydrogels have gained increasing attention in the field of biomedical applications,[54,72] but also usually a high concentration of GMA is required to guarantee printability. However, high concentrations of GMA can decrease cell viability, which calls for a reduction in its concentration for these hydrogels to become viable.[11] The gel phase of low-concentration GMA hydrogels does not have adequate mechanical strength to allow the structure to retain its initial geometry. Therefore, the central issue of GMA hydrogels in biomedical applications includes ensuring printability and biological functionality.[11,54,59] Here we seek to improve the mechanical resistance of GMA membranes by printing them on PLA fibrous mats obtained by the solution blow spinning technique. The values of modulus of elasticity, tensile strength, and elongation at the break of PLA fibrous mats and PLA/GMA, PLA/GMA/CD5, and PLA/GMA/CD10 membranes were obtained from stress−strain curves and are represented in Figure 5D−F, respectively. The results were compared with pure PLA mats, and all samples described a typical stress vs strain curve, where the first stages correspond to linear elastic behavior, followed by the nonlinear plastic region.

From the stress−strain curves it was possible to confirm a significant difference in the reduction of elastic modulus values of the PLA/GMA, PLA/GMA/CD5, and PLA/GMA/CD10 membranes (Figure 5D) when compared to the PLA fibrous mats, indicating a lower rigidity of these materials. Among the PLA/GMA, PLA/GMA/CD5, and PLA/GMA/CD10 membranes, a slight increase in the elastic modulus is observed with the increase in the concentration of CD to 10 wt %. The same behavior was observed for the tensile strength limit values (Figure 5E), that is, a significant reduction for the samples containing GMA when compared to the PLA fibrous mats. Concerning elongation (Figure 5F), an reversal was observed when comparing the membranes containing GMA with the PLA fibrous mat, that is, a more evident deformation was observed for the samples PLA/GMA, PLA/GMA/CD5, and PLA/GMA/CD10. Corroborating the behavior observed by the membranes in elongation at break, the SEM micrographs presented in Figure S4 illustrate the interaction between the GMA/CD-based hydrogel and the PLA nanofibers, where it is possible to observe that the nanofibers are well adhered to the

https://doi.org/10.1021/acsanm.4c03615
ACS Appl. Nano Mater. XXXX, XXX, XXX−XXX

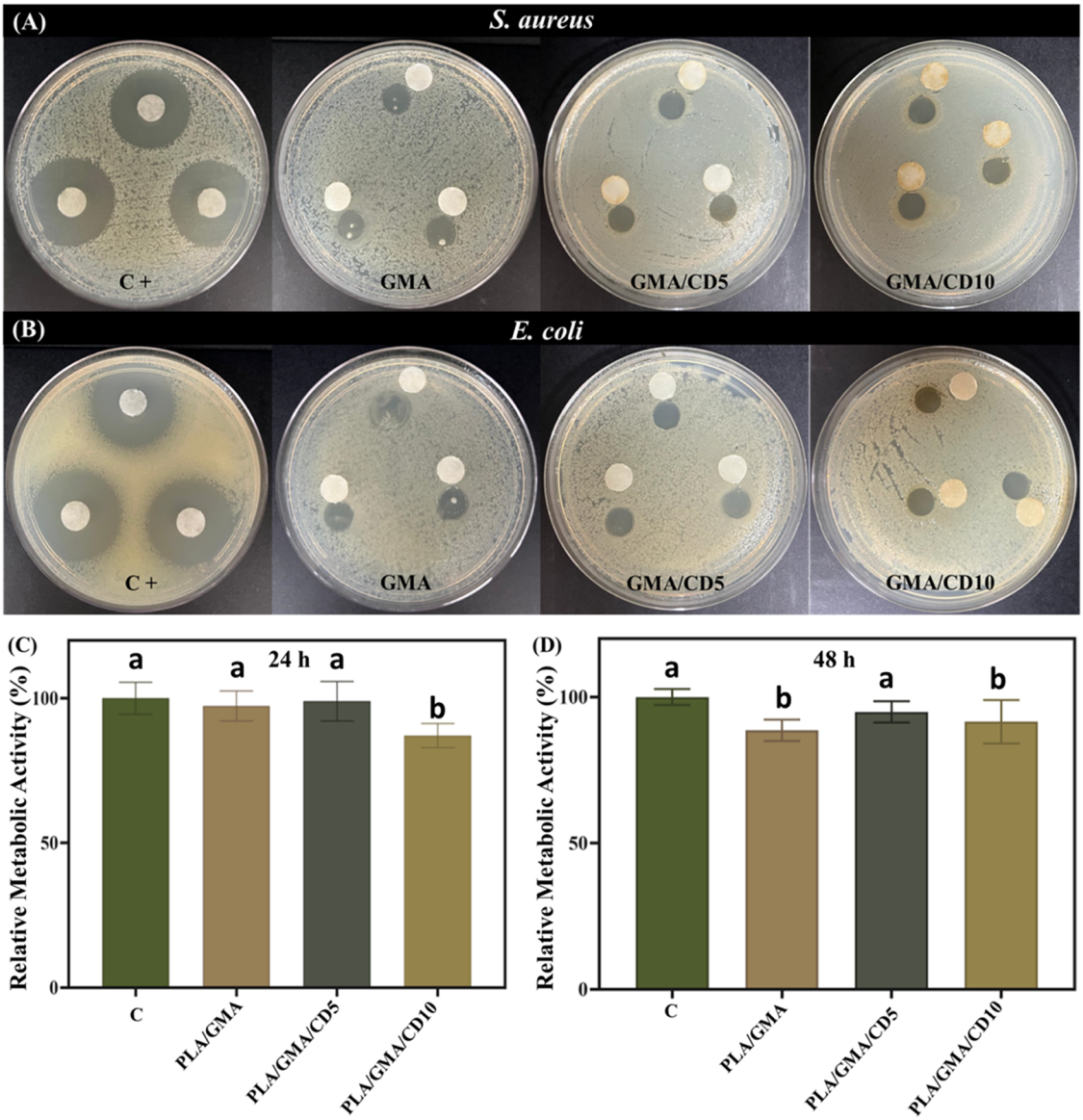

Figure 6. Antibacterial efficiency validated via disk diffusion assay for (A) *S. aureus* and (B) *E. coli*, where C+ refers to the positive control (Streptomycin Sulfate). Graphs of relative metabolic activity of fibroblasts analyzed with MTT assay, after 24 h (C) and 48 h (D) of exposure to the extract (results represented by mean ± standard deviation). Results that share (a and b) are statistically different by Tukey's test for $p < 0.05$.

hydrogel interface. This adhesion between the materials suggests that as the deformation was applied, the nanofibers were elongated until they reached the hydrogel, which in turn also began to elongate, creating a synergy between the materials, and contributing to the observed results in the elongation at break. Furthermore, Figures S2 and S3 in Supporting Information highlight the surface of the hydrogel after 3D printing and the morphology of the nanofibers produced by SBS. In general, the mechanical properties of the developed materials are similar to other results reported in the literature, both for the PLA fibrous mats,[39,73,74] as for GMA membranes, indicating that the presence of CDs did not significantly affect the mechanical behavior of the hydrogels.[25,59,75]

3.7. Disk Diffusion Antimicrobial Testing. *S. aureus* and *E. coli* are considered among the most prevalent pathogenic bacteria responsible for causing chronic wound-related infections.[76] Traditional dressings that are currently available on the market are generally presented as films, sponges, and foams. On the other hand, the development of multifunctional materials as replacements for common dressings is urgent due to the development of multiresistant strains of bacteria.[75] In this context, membranes composed of PLA fibrous mats and CDs-incorporated GMA can outperform classical drug delivery systems.[77] Therefore, we sought to evaluate the antimicrobial activity against *S. aureus* and *E. coli*, via the disk diffusion method, based on the hypothesis that membranes containing lignin carbon dots could be ideal dressing for local application in the wound region. For the analysis, hydrogels were used as membrane precursors, since GMA is thermosensitive and reaches its colloidal state at 37 °C.[11]

As shown in Figure 6A,B, no zones of inhibition were observed around the filters. However, all samples (excluding the control sample based on pure GMA) inhibited the ability of bacterial growth upon contact, which is a desirable feature for this type of application,[78] as confirmed for both bacterial strains tested. Furthermore, the presence of CDs may have contributed to the formation of physical or chemical

https://doi.org/10.1021/acsanm.4c03615
ACS Appl. Nano Mater. XXXX, XXX, XXX−XXX

interactions with the polymeric structure of GMA.[79−81] This interaction can hinder the diffusion of active compounds to the medium, consequently leading to the absence of an inhibition zone.[25] Specifically, the antibacterial activity of these materials can be attributed to the presence of lignin in the hydrogels, where the phenolic groups present in lignin are responsible for its antibacterial effect through oxidative stress and the ability to produce reactive oxygen species, resulting in the destabilization of the cell membrane.[82] Furthermore, lignin carbon dots are very sensitive to pH due to the ionization of surface functional groups, in particular, carboxylic acid groups, which demonstrate lower toxicity and better biocompatibility. Besides, they have many hydrophilic surface functional groups and disperse easily in aqueous media without additional surface modification.[81−85] These findings suggest that the 3D-printed membranes combined with bioactive compounds and fibrous mats are potentially useful for wound dressing applications.

3.8. Cytotoxicity Assay. To evaluate the potential cytotoxicity of membranes composed of GMA, the MTT assay was performed after 24 and 48 h of exposure of human fibroblasts to membrane extracts.[43,44] Three types of extracts were derived, namely PLA/GMA, PLA/GMA/CD5, and PLA/GMA/CD10, with the addition of a control group (exposed only to DMEM 10% SFB). The results shown in Figure 6C demonstrate that extracts for 24 h cannot modulate the metabolic activity of fibroblasts. Specifically, a decrease in cell viability of approximately 1.8, 2.53, and 9.02% was observed for the PLA/GMA, PLA/GMA/CD5, and PLA/GMA/CD10 groups, respectively. Although the ANOVA test indicates a significant difference among the groups, subsequent correction for multiple comparisons using Tukey's hypothesis test revealed no significant reduction between the control and the PLA/GMA and PLA/GMA/CD5 groups. Therefore, the only group displaying a significant reduction after 24 h of extracts was PLA/GMA/CD10. However, this reduction is insufficient to classify the material as cytotoxic according to ISO 10993-5/2009 standards, as the document specifies that the required reduction must exceed 30% to characterize cytotoxicity. During the preparation of extracts, two different incubation periods (24 and 48 h) between the membranes and the medium were utilized. It is noteworthy that the 48 h incubation period has the potential to yield an extract with a higher concentration of material components. This can underscore the potential impact of prolonged material release on cell viability. The cytotoxicity of 48 h extract is shown in Figure 6D. A reduction in cell viability of 5.32, 1.48, and 4.97% was observed for the PLA/GMA, PLA/GMA/CD5, and PLA/GMA/CD10 groups, respectively, which was corroborated by the one-way ANOVA test ($p < 0.05$). Correction for multicomparison using Tukey's hypothesis test revealed the absence of a significant reduction between the control and the PLA/GMA/CD5 group only. Although the PLA/GMA and PLA/GMA/CD10 groups present a significant reduction concerning the control, this is not enough to constitute cytotoxicity to the material according to ISO 10993-5/2009. This underscores that GMA membranes did not alter the metabolic activity of fibroblasts, even after exposure to 48 h extracts of the material. Therefore, these results indicate that membranes composed of the fibrous layer of PLA and GMA, even when associated with CDs, do not cause relevant cytotoxic effects in human fibroblasts, indicating that these membranes have cytocompatibility, and are probably a safe product and a promising alternative to wound dressing. Finally, it is also important to emphasize that the concentration of Irgacure 2959 employed in the cross-linking of the GMA-based membranes did not present cytotoxicity for the fibroblasts used in the *in vitro* assays. Additionally, it facilitated the production of materials (Figure 4F−H) with potential for wound dressing applications.

4. CONCLUSIONS

We developed a multifunctional wound dressing using methacrylated gelatin (GMA) incorporated with lignin carbon dots (CDs) processed by 3D printing, which was deposited on the top of PLA fibrous mats fabricated by solution blow spinning. Our results indicate that the incorporation of lignin CDs imparted antimicrobial properties against *S. aureus* and *E. coli* to the hydrogel, without significantly altering the structure of the GMA-based membranes. Furthermore, the combination of GMA membranes and PLA fibrous mats exhibited favorable mechanical properties, such as remarkable capacity of mechanical deformability and ability to maintain a hydrated environment with controlled degradation. In addition, cytotoxicity studies revealed no adverse effects on the tested human cells, suggesting biocompatibility, although *in vivo* tests is needed for confirmation. Moreover, as the wound dressing contains lignin CDs with fluorescent and electrical properties, these can be explored in future studies for potential use in wearable electrical sensors or sensing materials capable of detecting microorganisms via fluorescence signals. In summary, our findings suggest that the developed material paves the way for manufacturing novel multifunction wound dressings for biomedical applications, taking advantage of biodegradable and sustainable nanomaterials that can be manufactured in a simple way.

■ ASSOCIATED CONTENT

Data Availability Statement

Data will be made available on request.

Supporting Information

The Supporting Information is available free of charge at https://pubs.acs.org/doi/10.1021/acsanm.4c03615.

Physicochemical characterizations of lignin carbon dots, including fluorescence and UV−vis spectroscopies, and transmission electron microscopy (TEM). SEM micrographs of the 3D-printed hydrogel on the top of PLA nanofibers, the PLA nanofibers obtained by SBS and the interface region of the PLA nanofibers/GMA/CD-based hydrogel membrane (PDF)

■ AUTHOR INFORMATION

Corresponding Authors

Rodrigo L. Oréfice − *Department of Metallurgical and Materials Engineering, Federal University of Minas Gerais, 31270-901 Belo Horizonte, Brazil;* orcid.org/0000-0002-6046-4056; Email: rorefice@demet.ufmg.br

Daniel S. Correa − *Nanotechnology National Laboratory for Agriculture (LNNA), Embrapa Instrumentation, 13560-970 Sao Carlos, SP, Brazil; Materials Engineering Department, Sao Carlos School of Engineering, University of Sao Paulo, 13563-120 Sao Carlos, SP, Brazil; PPGQ, Department of Chemistry, Center for Exact Sciences and Technology, Federal University of São Carlos (UFSCar), 13565-905 São Carlos, SP, Brazil;* orcid.org/0000-0002-5592-0627; Email: daniel.correa@embrapa.br

https://doi.org/10.1021/acsanm.4c03615
ACS Appl. Nano Mater. XXXX, XXX, XXX−XXX

Authors

Patrícia F. Rossi − *Department of Metallurgical and Materials Engineering, Federal University of Minas Gerais, 31270-901 Belo Horizonte, Brazil; Nanotechnology National Laboratory for Agriculture (LNNA), Embrapa Instrumentation, 13560-970 Sao Carlos, SP, Brazil;* orcid.org/0009-0002-5701-4262

Francisco Vieira dos Santos − *Nanotechnology National Laboratory for Agriculture (LNNA), Embrapa Instrumentation, 13560-970 Sao Carlos, SP, Brazil; Materials Engineering Department, Sao Carlos School of Engineering, University of Sao Paulo, 13563-120 Sao Carlos, SP, Brazil;* orcid.org/0000-0003-1258-2821

Ana Laura Martins Mulkson Alves − *Nanotechnology National Laboratory for Agriculture (LNNA), Embrapa Instrumentation, 13560-970 Sao Carlos, SP, Brazil; PPGQ, Department of Chemistry, Center for Exact Sciences and Technology, Federal University of São Carlos (UFSCar), 13565-905 São Carlos, SP, Brazil*

Leonardo Henrique Semensato − *Nanotechnology National Laboratory for Agriculture (LNNA), Embrapa Instrumentation, 13560-970 Sao Carlos, SP, Brazil; Sao Carlos Institute of Chemistry, University of Sao Paulo, 13566-590 Sao Carlos, SP, Brazil;* orcid.org/0000-0002-8674-1517

Luis Fernando Rocha Oliveira − *Nanotechnology National Laboratory for Agriculture (LNNA), Embrapa Instrumentation, 13560-970 Sao Carlos, SP, Brazil*

Danilo M. dos Santos − *Nanotechnology National Laboratory for Agriculture (LNNA), Embrapa Instrumentation, 13560-970 Sao Carlos, SP, Brazil;* orcid.org/0000-0002-3884-3236

Tiago de Paula Bianchi − *Sao Carlos Institute of Physics, University of Sao Paulo, 13566-590 Sao Carlos, SP, Brazil*

Natália M. Inada − *Sao Carlos Institute of Physics, University of Sao Paulo, 13566-590 Sao Carlos, SP, Brazil*

Sérgio Paulo Campana-Filho − *Sao Carlos Institute of Chemistry, University of Sao Paulo, 13566-590 Sao Carlos, SP, Brazil;* orcid.org/0000-0002-0980-0085

Complete contact information is available at: https://pubs.acs.org/10.1021/acsanm.4c03615

Funding

The Article Processing Charge for the publication of this research was funded by the Coordination for the Improvement of Higher Education Personnel - CAPES (ROR identifier: 00x0ma614).

Notes

The authors declare no competing financial interest.

■ ACKNOWLEDGMENTS

The authors thank the Conselho Nacional de Desenvolvimento Científico e Tecnológico (CNPq) (140681/2020-5) and (311464/2022-0), Fundação de Amparo à Pesquisa do Estado de São Paulo (FAPESP) (2022/05316-5, 2018/22214-6, 2013/07276-1), Coordenação de Aperfeiçoamento de Pessoal de Nível Superior (CAPES) from Brazil for financial support.

■ REFERENCES

(1) Khoshmaram, K.; Yazdian, F.; Pazhouhnia, Z.; Lotfibakhshaiesh, N. Preparation and Characterization of 3D Bioprinted Gelatin Methacrylate Hydrogel Incorporated with Curcumin Loaded Chitosan Nanoparticles for in Vivo Wound Healing Application. *Biomater. Adv.* **2024**, *156*, No. 213677.

(2) Las Heras, K.; Igartua, M.; Santos-Vizcaino, E.; Hernandez, R. M. Chronic Wounds: Current Status, Available Strategies and Emerging Therapeutic Solutions. *J. Controlled Release* **2020**, *328*, 532−550.

(3) Sun, Y.; Juncos Bombin, A. D.; Boyd, P.; Dunne, N.; McCarthy, H. O. Application of 3D Printing & 3D Bioprinting for Promoting Cutaneous Wound Regeneration. *Bioprinting* **2022**, *28*, No. e00230.

(4) Wang, Y.; Yuan, X.; Yao, B.; Zhu, S.; Zhu, P.; Huang, S. Tailoring Bioinks of Extrusion-Based Bioprinting for Cutaneous Wound Healing. *Bioact. Mater.* **2022**, *17*, 178−194.

(5) Sharifi, S.; Hajipour, M. J.; Gould, L.; Mahmoudi, M. Nanomedicine in Healing Chronic Wounds: Opportunities and Challenges. *Mol. Pharmaceutics.* **2021**, *18* (2), 550−575.

(6) Ambekar, R. S.; Kandasubramanian, B. Advancements in Nanofibers for Wound Dressing: A Review. *Eur. Polym. J.* **2019**, *117*, 304−336.

(7) Borda, L. J.; Macquhae, F. E.; Kirsner, R. S. Wound Dressings: A Comprehensive Review. *Curr. Dermatol. Rep.* **2016**, *5*, 287−297.

(8) Memic, A.; Abudula, T.; Mohammed, H. S.; Joshi Navare, K.; Colombani, T.; Bencherif, S. A. Latest Progress in Electrospun Nanofibers for Wound Healing Applications. *ACS Appl. Bio Mater.* **2019**, *2*, 952−969.

(9) Qu, J.; Zhao, X.; Liang, Y.; Zhang, T.; Ma, P. X.; Guo, B. Antibacterial Adhesive Injectable Hydrogels with Rapid Self-Healing, Extensibility and Compressibility as Wound Dressing for Joints Skin Wound Healing. *Biomaterials* **2018**, *183*, 185−199.

(10) Mirek, A.; Belaid, H.; Bartkowiak, A.; Barranger, F.; Salmeron, F.; Kajdan, M.; Grzeczkowicz, M.; Cavaillès, V.; Lewińska, D.; Bechelany, M. Gelatin Methacrylate Hydrogel with Drug-Loaded Polymer Microspheres as a New Bioink for 3D Bioprinting. *Biomater. Adv.* **2023**, *150*, No. 213436.

(11) Xu, L.; Zhang, Z.; Jorgensen, A. M.; Yang, Y.; Jin, Q.; Zhang, G.; Cao, G.; Fu, Y.; Zhao, W.; Ju, J.; Hou, R. Bioprinting a Skin Patch with Dual-Crosslinked Gelatin (GelMA) and Silk Fibroin (SilMA): An Approach to Accelerating Cutaneous Wound Healing. *Mater. Today. Bio.* **2023**, *18*, No. 100550.

(12) Ligon, S. C.; Liska, R.; Stampfl, J.; Gurr, M.; Mülhaupt, R. Polymers for 3D Printing and Customized Additive Manufacturing. *Chem. Rev.* **2017**, *117*, 10212−10290.

(13) Mitchell, A.; Lafont, U.; Hołyńska, M.; Semprimoschnig, C. Additive Manufacturing — A Review of 4D Printing and Future Applications. *Addit. Manuf.* **2018**, *24*, 606−626.

(14) Bedell, M. L.; Navara, A. M.; Du, Y.; Zhang, S.; Mikos, A. G. Polymeric Systems for Bioprinting. *Chem. Rev.* **2020**, *120*, 10744−10792.

(15) Singh, S.; Ramakrishna, S.; Singh, R. Material Issues in Additive Manufacturing: A Review. *J. Manuf. Process.* **2017**, *25*, 185−200.

(16) Zhang, Y.; Yu, J.; Zhang, H.; Li, Y.; Wang, L. Nanofibrous Dressing: Potential Alternative for Fighting against Antibiotic-Resistance Wound Infections. *J. Appl. Polym. Sci.* **2022**, *139*, No. e52178.

(17) Fayyazbakhsh, F.; Khayat, M. J.; Leu, M. C. 3D-Printed Gelatin-Alginate Hydrogel Dressings for Burn Wound Healing: A Comprehensive Study. *Int. J. Bioprint.* **2022**, *8* (4), 274−291.

(18) Long, J.; Etxeberria, A. E.; Nand, A. V.; Bunt, C. R.; Ray, S.; Seyfoddin, A. A 3D Printed Chitosan-Pectin Hydrogel Wound Dressing for Lidocaine Hydrochloride Delivery. *Mater. Sci. Eng. C* **2019**, *104*, No. 109873.

(19) Souza, S. O. L. d.; de Oliveira, S. M.; Lehman, C. P.; da Silva, M. C.; Silva, L. M.; Oréfice, R. L. Tuning the Structure and Properties of Cell-Embedded Gelatin Hydrogels for Tumor Organoids. *Polimeros* **2023**, *33* (2), No. e20230014, DOI: 10.1590/0104-1428.20220024.

(20) Aldana, A. A.; Valente, F.; Dilley, R.; Doyle, B. Development of 3D Bioprinted GelMA-Alginate Hydrogels with Tunable Mechanical Properties. *Bioprinting* **2021**, *21*, No. e00105.

(21) Iervolino, F.; Belgio, B.; Bonessa, A.; Potere, F.; Suriano, R.; Boschetti, F.; Mantero, S.; Levi, M. Versatile and Non-Cytotoxic GelMA-Xanthan Gum Biomaterial Ink for Extrusion-Based 3D Bioprinting. *Bioprinting* **2023**, *31*, No. e00269.
(22) Jin, R.; Cui, Y.; Chen, H.; Zhang, Z.; Weng, T.; Xia, S.; Yu, M.; Zhang, W.; Shao, J.; Yang, M.; Han, C.; Wang, X. Three-Dimensional Bioprinting of a Full-Thickness Functional Skin Model Using Acellular Dermal Matrix and Gelatin Methacrylamide Bioink. *Acta. Biomater.* **2021**, *131*, 248−261.
(23) Rastin, H.; Ormsby, R. T.; Atkins, G. J.; Losic, D. 3D Bioprinting of Methylcellulose/Gelatin-Methacryloyl (MC/GelMA) Bioink with High Shape Integrity. *ACS. Appl. Bio. Mater.* **2020**, *3* (3), 1815−1826.
(24) Yu, O.; Kim, K. H. Lignin to Materials: A Focused Review on Recent Novel Lignin Applications. *Appl. Sci.* **2020**, *10* (13), 4626.
(25) Zhang, T.; Li, H.; Zhou, J.; Wang, X.; Xiao, L.; Zhang, F.; Guo, Y. Review of Carbon Dots from Lignin: Preparing, Tuning, and Applying. *Pap. Biomater.* **2022**, *7* (3), 51−62.
(26) Chen, W.; Hu, C.; Yang, Y.; Cui, J.; Liu, Y. Rapid Synthesis of Carbon Dots by Hydrothermal Treatment of Lignin. *Materials* **2016**, *9* (3), 184.
(27) Zhang, B.; Liu, Y.; Ren, M.; Li, W.; Zhang, X.; Vajtai, R.; Ajayan, P. M.; Tour, J. M.; Wang, L. Sustainable Synthesis of Bright Green Fluorescent Nitrogen-Doped Carbon Quantum Dots from Alkali Lignin. *Chem. Sus. Chem.* **2019**, *12* (18), 4202−4210.
(28) Wang, J.; Wang, J.; Xiao, W.; Geng, Z.; Tan, D.; Wei, L.; Li, J.; Xue, L.; Wang, X.; Zhu, J. Lignin-Derived Red-Emitting Carbon Dots for Colorimetric and Sensitive Fluorometric Detection of Water in Organic Solvents. *Anal. Methods* **2020**, *12* (25), 3218−3224.
(29) Ding, Z.; Li, F.; Wen, J.; Wang, X.; Sun, R. Gram-Scale Synthesis of Single-Crystalline Graphene Quantum Dots Derived from Lignin Biomass. *Green. Chem.* **2018**, *20* (6), 1383−1390.
(30) Duarte, É. C.; Oréfice, R. L. Self-Healing Interfaces of Poly(Methyl Methacrylate) Reinforced with Carbon Fibers Decorated with Carbon Quantum Dots. *J. Appl. Polym. Sci.* **2021**, *138* (1), No. e49644.
(31) Liu, W.; Ning, C.; Sang, R.; Hou, Q.; Ni, Y. Lignin-Derived Graphene Quantum Dots from Phosphous Acid-Assisted Hydrothermal Pretreatment and Their Application in Photocatalysis. *Ind. Crops. Prod.* **2021**, *171*, No. 113963.
(32) Sk, M. P.; Dutta, A. New-Generation Quantum Dots as Contrast Agent in Imaging. *Nanomater. Diagn. Tools Devices* **2020**, *18*, 525−556.
(33) Xiao, T.; Wang, Y.; Wang, H.; Zhang, Y.; Zhou, J.; Zhao, Q. Anticoagulant and antioxidant properties of hemodialysis membranes modified by hydrogels incorporating carbon dots. *J. Membr. Sci.* **2024**, *692*, No. 122318.
(34) Ramanadha reddy, S.; Venkatachalapathi, N., Dr. A Review on Characteristic Variation in PLA Material with a Combination of Various Nano Composites *Mater. Today. Proc.* 2023, DOI: 10.1016/j.matpr.2023.04.616.
(35) Abdenour, C.; Eesaee, M.; Stuppa, C.; Chabot, B.; Barnabé, S.; Bley, J.; Tolnai, B.; Guy, N.; Nguyen-Tri, P. Water Vapor and Air Barrier Performance of Sustainable Paper Coatings Based on PLA and Xanthan Gum. *Mater.Today. Commun.* **2023**, *36*, No. 106626.
(36) Arthanari, S.; Park, J. E.; Heo, J. S.; Cho, D. H.; Yang, M.; Hwang, J. S.; Lee, H. Laser Surface Polishing of 3D Printed Polylactic Acid (PLA) with Different Levels of Absorption. *J. Manuf. Process.* **2023**, *98*, 265−276.
(37) Schneider, R.; Facure, M. H. M.; Alvarenga, A. D.; Chagas, P. A. M.; Dos Santos, D. M.; Correa, D. S. Dye Adsorption Capacity of MoS_2 Nanoflakes Immobilized on Poly(Lactic Acid) Fibrous Membranes. *ACS. Appl. Nano. Mater.* **2021**, *4* (5), 4881−4894.
(38) Sun, S.; Gao, L.; Liang, B.; Yin, Z.; Pan, S.; Shi, C.; Guo, C.; Huang, Z.; Chu, C.; Dong, Y. Long-Term and Uniform Release of Magnesium Ions from PLA Porous Composite Materials Oriently Reinforced by Mg Wires for Potential Bone Repair Application. *Surf. Interfaces* **2023**, *40*, No. 103018.
(39) Grizzo, A.; dos Santos, D. M.; da Costa, V. P. V.; Lopes, R. G.; Inada, N. M.; Correa, D. S.; Campana-Filho, S. P. Multifunctional Bilayer Membranes Composed of Poly(Lactic Acid), Beta-Chitin Whiskers and Silver Nanoparticles for Wound Dressing Applications. *Int. J. Biol. Macromol.* **2023**, *251*, No. 126314.
(40) Zhu, S.; Yu, C.; Liu, N.; Zhao, M.; Chen, Z.; Liu, J.; Li, G.; Huang, H.; Guo, H.; Sun, T.; Chen, J.; Zhuang, J.; Zhu, P. Injectable Conductive Gelatin Methacrylate/Oxidized Dextran Hydrogel Encapsulating Umbilical Cord Mesenchymal Stem Cells for Myocardial Infarction Treatment. *Bioact. Mater.* **2022**, *13*, 119−134.
(41) Baigorria, E.; Souza dos Santos, S.; de Moura, M. R.; Fraceto, L. F. Nanocomposite Hydrogels 3D Printed for Application in Water Remediation. *Mater. Today. Chem.* **2023**, *30*, No. 101559.
(42) Stie, M. B.; Gätke, J. R.; Wan, F.; Chronakis, I. S.; Jacobsen, J.; Nielsen, H. M. Swelling of Mucoadhesive Electrospun Chitosan/Polyethylene Oxide Nanofibers Facilitates Adhesion to the Sublingual Mucosa. *Carbohydr. Polym.* **2020**, *242*, No. 116428.
(43) Corrales-Orovio, R.; Carvajal, F.; Holmes, C.; Miranda, M.; González-Itier, S.; Cárdenas, C.; Vera, C.; Schenck, T. L.; Egaña, J. T. Development of a Photosynthetic Hydrogel as Potential Wound Dressing for the Local Delivery of Oxygen and Bioactive Molecules. *Acta Biomater.* **2023**, *155*, 154−166.
(44) Min, D.; Ahn, Y.; Lee, H. K.; Jung, W.; Kim, H. J. A Novel Optical Coherence Tomography-Based in Vitro Method of Anti-Aging Skin Analysis Using 3D Skin Wrinkle Mimics. *Sking Res. Technol.* **2023**, *29* (6), No. e13354.
(45) Xiong, J.; Grace, M. H.; Kobayashi, H.; Lila, M. A. Evaluation of Saffron Extract Bioactivities Relevant to Skin Resilience. *J. Herb. Med.* **2023**, *37*, No. 100629.
(46) Wu, C. S.; Hsu, Y. C.; Liao, H. T.; Cai, Y. X. Antibacterial Activity and in Vitro Evaluation of the Biocompatibility of Chitosan-Based Polysaccharide/Polyester Membranes. *Carbohydr. Polym.* **2015**, *134*, 438−447.
(47) Bercea, M. Rheology as a Tool for Fine-Tuning the Properties of Printable Bioinspired Gels. *Molecules* **2023**, *28* (6), 2766.
(48) Stojkov, G.; Niyazov, Z.; Picchioni, F.; Bose, R. K. Relationship between Structure and Rheology of Hydrogels for Various Applications. *Gels* **2021**, *7* (4), 255.
(49) Fundarò, S. P.; Salti, G.; Malgapo, D. M. H.; Innocenti, S. The Rheology and Physicochemical Characteristics of Hyaluronic Acid Fillers: Their Clinical Implications. *Int. J. Mol. Sci.* **2022**, *23* (18), 10518.
(50) Hoffman, A. S. Hydrogels for Biomedical Applications. *Adv. Drug. Delivery Rev.* **2012**, *64*, 18−23.
(51) Gao, T.; Gillispie, G. J.; Copus, J. S.; Kumar, A. P. R.; Seol, Y. J.; Atala, A.; Yoo, J. J.; Lee, S. J. Optimization of Gelatin-Alginate Composite Bioink Printability Using Rheological Parameters: A Systematic Approach. *Biofabrication* **2018**, *10* (3), No. 034106.
(52) Herrada-Manchón, H.; Fernández, M. A.; Aguilar, E. Essential Guide to Hydrogel Rheology in Extrusion 3D Printing: How to Measure It and Why It Matters? *Gels* **2023**, *9* (7), 517.
(53) Amorim, P. A.; d'Ávila, M. A.; Anand, R.; Moldenaers, P.; Van Puyvelde, P.; Bloemen, V. Insights on Shear Rheology of Inks for Extrusion-Based 3D Bioprinting. *Bioprinting* **2021**, *22*, No. e00129.
(54) Yin, J.; Yan, M.; Wang, Y.; Fu, J.; Suo, H. 3D Bioprinting of Low-Concentration Cell-Laden Gelatin Methacrylate (GelMA) Bioinks with a Two-Step Cross-Linking Strategy. *ACS Appl. Mater. Interfaces* **2018**, *10* (8), 6849−6857.
(55) Townsend, J. M.; Beck, E. C.; Gehrke, S. H.; Berkland, C. J.; Detamore, M. S. Flow Behavior Prior to Crosslinking: The Need for Precursor Rheology for Placement of Hydrogels in Medical Applications and for 3D Bioprinting. *Prog. Polym. Sci.* **2019**, *91*, 126−140.
(56) Paxton, N.; Smolan, W.; Böck, T.; Melchels, F.; Groll, J.; Jungst, T. Proposal to Assess Printability of Bioinks for Extrusion-Based Bioprinting and Evaluation of Rheological Properties Governing Bioprintability. *Biofabrication* **2017**, *9* (4), No. 044107.
(57) Bom, S.; Ribeiro, R.; Ribeiro, H. M.; Santos, C.; Marto, J. On the Progress of Hydrogel-Based 3D Printing: Correlating Rheological

https://doi.org/10.1021/acsanm.4c03615
ACS Appl. Nano Mater. XXXX, XXX, XXX−XXX

Properties with Printing Behaviour. *Int. J. Pharm.* **2022**, *615*, No. 121506.
(58) Chen, X.; Zhang, D.; Wang, X.; Liu, Z.; Kang, H.; Liu, C.; Chen, F. Preparation of Porous GelMA Microcarriers by Microfluidic Technology for Stem-Cell Culture. *Chem. Eng. J.* **2023**, *477*, No. 146444.
(59) Lee, B. H.; Lum, N.; Seow, L. Y.; Lim, P. Q.; Tan, L. P. Synthesis and Characterization of Types A and B Gelatin Methacryloyl for Bioink Applications. *Materials* **2016**, *9* (10), 797.
(60) Zhu, M.; Wang, Y.; Ferracci, G.; Zheng, J.; Cho, N. J.; Lee, B. H. Gelatin Methacryloyl and Its Hydrogels with an Exceptional Degree of Controllability and Batch-to-Batch Consistency. *Sci. Rep.* **2019**, *9* (1), No. 6863, DOI: 10.1038/s41598-019-42186-x.
(61) Leu Alexa, R.; Iovu, H.; Ghitman, J.; Serafim, A.; Stavarache, C.; Marin, M. M.; Ianchis, R. 3D-Printed Gelatin Methacryloyl-Based Scaffolds with Potential Application in Tissue Engineering. *Polymers* **2021**, *13* (5), 727.
(62) Rahali, K.; Ben Messaoud, G.; Kahn, C. J. F.; Sanchez-Gonzalez, L.; Kaci, M.; Cleymand, F.; Fleutot, S.; Linder, M.; Desobry, S.; Arab-Tehrany, E. Synthesis and Characterization of Nanofunctionalized Gelatin Methacrylate Hydrogels. *Int. J. Mol. Sci.* **2017**, *18* (12), 2675.
(63) Sun, M.; Sun, X.; Wang, Z.; Guo, S.; Yu, G.; Yang, H. Synthesis and Properties of Gelatin Methacryloyl (GelMA) Hydrogels and Their Recent Applications in Load-Bearing Tissue. *Polymers* **2018**, *10* (11), 1290.
(64) Krishnamoorthy, S.; Noorani, B.; Xu, C. Effects of Encapsulated Cells on the Physical−Mechanical Properties and Microstructure of Gelatin Methacrylate Hydrogels. *Int. J. Mol. Sci.* **2019**, *20* (20), 5061.
(65) Cassales, A.; Ramos, L. A.; Frollini, E. Synthesis of Bio-Based Polyurethanes from Kraft Lignin and Castor Oil with Simultaneous Film Formation. *Int. J. Biol. Macromol.* **2020**, *145*, 28−41.
(66) Teshima, R.; Osawa, S.; Yoshikawa, M.; Kawano, Y.; Otsuka, H.; Hanawa, T. Low-Adhesion and Low-Swelling Hydrogel Based on Alginate and Carbonated Water to Prevent Temporary Dilation of Wound Sites. *Int. J. Biol. Macromol.* **2024**, *254*, No. 127928.
(67) Ravikumar, R.; Ganesh, M.; Ubaidulla, U.; Young Choi, E.; Tae Jang, H. Preparation, Characterization, and in Vitro Diffusion Study of Nonwoven Electrospun Nanofiber of Curcumin-Loaded Cellulose Acetate Phthalate Polymer. *Saudi Pharm. J.* **2017**, *25* (6), 921−926.
(68) Zhou, C.; Sheng, C.; Chen, J.; Liang, Y.; Liu, Q.; Li, P.; Huang, X.; Liu, B. Gradual hydrogel degradation for programable repairing full-thickness skin defect wound. *Chem. Eng. J.* **2022**, *450* (3), No. 138200.
(69) Chen, H.; Li, B.; Feng, B.; Wang, H.; Yuan, H.; Xu, Z. Tetracycline Hydrochloride Loaded Citric Acid Functionalized Chitosan Hydrogel for Wound Healing. *RSC. Adv.* **2019**, *9* (34), 19523−19530.
(70) Nwomeh, B. C.; Liang, H.-X.; Cohen, I. K.; Yager, D. R. MMP-8 Is the Predominant Collagenase in Healing Wounds and Nonhealing Ulcers. *J. Surg. Res.* **1999**, *81* (2), 189−195.
(71) Zhao, Y.; Dai, C.; Wang, Z.; Chen, W.; Liu, J.; Zhuo, R.; Yu, A.; Huang, S. A Novel Curcumin-Loaded Composite Dressing Facilitates Wound Healing Due to Its Natural Antioxidant Effect. *Drug Des., Dev. Ther.* **2019**, *13*, 3269−3280.
(72) Zhang, Y.; Lv, J.; Zhao, J.; Ling, G.; Zhang, P. A Versatile GelMA Composite Hydrogel: Designing Principles, Delivery Forms and Biomedical Applications. *Eur. Polym. J.* **2023**, *197*, No. 112370.
(73) Krasian, T.; Punyodom, W.; Molloy, R.; Topham, P. D.; Tighe, B. J.; Mahomed, A.; Chaiwarit, T.; Panraksa, P.; Rachtanapun, P.; Jantanasakulwong, K.; Worajittiphon, P. Low Cytotoxicity, Antibacterial Property, and Curcumin Delivery Performance of Toughness-Enhanced Electrospun Composite Membranes Based on Poly(Lactic Acid) and MAX Phase (Ti_3AlC_2). *Int. J. Biol. Macromol.* **2024**, *262*, No. 129967.
(74) Ramdhanie, L. I.; Aubuchon, S. R.; Boland, E. D.; Knapp, D. C.; Barnes, C. P.; Simpson, D. G.; Wnek, G. E.; Bowlin, G. L. Thermal and Mechanical Characterization of Electrospun Blends of Poly(Lactic Acid) and Poly(Glycolic Acid). *Polym. J.* **2006**, *38* (11), 1137−1145.
(75) Guo, A.; Zhang, S.; Yang, R.; Sui, C. Enhancing the Mechanical Strength of 3D Printed GelMA for Soft Tissue Engineering Applications. *Mater. Today Bio* **2024**, *24*, No. 100939.
(76) Sachdeva, C.; Satyamoorthy, K.; Murali, T. S. Microbial Interplay in Skin and Chronic Wounds. *Curr. Clin. Microbiol. Rep.* **2022**, *9*, 21−31.
(77) Homaeigohar, S.; Boccaccini, A. R. Antibacterial Biohybrid Nanofibers for Wound Dressings. *Acta Biomater.* **2020**, *107*, 25−49.
(78) Dhivya, S.; Padma, V. V.; Santhini, E. Wound Dressings - A Review. *BioMedicine* **2015**, *5* (5), 24−28.
(79) Aggarwal, M.; Panigrahi, H.; Kotnees, D. K.; Das, P. Multifunctional Self-Healing Carbon Dot-Gelatin Bioadhesive: Improved Tissue Adhesion with Simultaneous Drug Delivery, Optical Tracking, and Photoactivated Sterilization. *Biomacromolecules* **2024**, *25* (5), 3178−3189.
(80) Li, K.; Zhong, W.; Li, P.; Ren, J.; Jiang, K.; Wu, W. Antibacterial Mechanism of Lignin and Lignin-Based Antimicrobial Materials in Different Fields. *Int. J. Biol. Macromol.* **2023**, *252*, No. 126281.
(81) Morena, A. G.; Tzanov, T. Antibacterial Lignin-Based Nanoparticles and Their Use in Composite Materials. *Nanoscale Adv.* **2022**, *4*, 4447−4469.
(82) Li, Y.; Hu, M.; Liu, K.; Gao, S.; Lian, H.; Xu, C. Lignin Derived Multicolor Carbon Dots for Visual Detection of Formaldehyde. *Ind. Crops Prod.* **2023**, *192*, No. 116006.
(83) Ehtesabi, H.; Hallaji, Z.; Najafi Nobar, S.; Bagheri, Z. Carbon Dots with PH-Responsive Fluorescence: A Review on Synthesis and Cell Biological Applications. *Microchim. Acta.* **2020**, *187*, 150.
(84) Marangon, C. A.; Otoni, C. G.; Bertuso, P. C.; Rossi, P. F.; dos Santos, D. M.; Lourençon, T. V.; Martins, V. C. A.; Plepis, A. M. G.; Mattoso, L. H. C.; Nitschke, M. Side-Stream Lignins: Potential Antioxidant and Antimicrobial Agents in Milk. *Food. Res. Int.* **2024**, *180*, No. 114091.
(85) Morena, A. G.; Bassegoda, A.; Natan, M.; Jacobi, G.; Banin, E.; Tzanov, T. Antibacterial Properties and Mechanisms of Action of Sonoenzymatically Synthesized Lignin-Based Nanoparticles. *ACS Appl. Mater. Interfaces* **2022**, *14* (33), 37270−37279.

https://doi.org/10.1021/acsanm.4c03615
ACS Appl. Nano Mater. XXXX, XXX, XXX−XXX